An Adaptive Integral Backstepping SMC and Robust Functional Expanded Multikernel BLS Based MPPT Control in PV-Battery DC Microgrid System

Mrutyunjaya Sahani, *Senior Member, IEEE*, Baladev Biswal, *Student Member, IEEE*, Eluri NVDV Prasad, *Member, IEEE*, Pradipta Kishore Dash, *Life Senior Member, IEEE*, and Sanjib Kumar Panda, *Fellow, IEEE*

***Abstract*—In this article, a robust functional expanded multikernel broad learning system (RFEMBLS) is proposed to compute the complex nonlinear solar photovoltaic (PV) reference voltage more accurately by importing the irradiance and temperature in different uncertainty conditions. The novel droop control mechanism is introduced to obtain reference current to reduce dependence on different connected renewable energy resources. An adaptive integral backstepping sliding mode controller (AIBSMC) is designed to control the dc bus voltage under different abnormal scenarios for the proposed dc microgrid. An asymptotical stability analysis is developed using Lyapunov theory for the PV-battery dc microgrid. A new adoption rule is proposed for the estimation of both references of PV voltage and battery current. Furthermore, the system steady-state error and tracking convergence of the error are improved by adding an integral action. The backstepping method based on the dc bus voltage feedback results in a faster response and negligible chattering. A sliding mode controller is proposed to improve the control precision and robustness. Finally, the proposed RFEMBLS-AIBSMC method is tested using dSPACE platform in the scale-down lab environment to verify the robustness, practicability, feasibility, and efficacy of the proposed system in the real-time scenario.**

***Index Terms*—Adaptive integral backstepping sliding mode control, DSPACE hardware in loop, functional expanded broad learning system, kernel learning, Lyapunov criteria, maximum power point tracking, photovoltaic.**

Manuscript received 27 June 2023; revised 29 September 2023; accepted 29 October 2023. Date of publication 14 November 2023; date of current version 26 January 2024. This work was supported by the National Research Foundation, Singapore, jointly with Energy Market Authority and Keppel Offshore & Marine Limited under the Energy Programme "EMA-KOM Joint RFP (EMA-EP007-EKOM)" with Envision Digital International Pte. Ltd. as the main Host Institution. Recommended for publication by Associate Editor Li (SSGAE_M) Peng. *(Corresponding author: Sanjib Kumar Panda.)*

Mrutyunjaya Sahani and Sanjib Kumar Panda are with the Department of Electrical and Computer Engineering, National University of Singapore, Singapore 119077 (e-mail: mrutyunjayasahane@gmail.com; eleskp@nus.edu.sg).

Baladev Biswal and Pradipta Kishore Dash are with Multidisciplinary Research Cell, Siksha 'O' Anusandhan Deemed to be University, Bhubaneswar 751030, India (e-mail: biswalbaladev@gmail.com; pkdash.india@gmail.com).

Eluri NVDV Prasad is with the Department of Electrical Engineering, Sri Vasavi Engineering Autonomous College, Tadepalligudem 534101, India (e-mail: varaprasadeee20@gmail.com).

Color versions of one or more figures in this article are available at https://doi.org/10.1109/TPEL.2023.3332641.

Digital Object Identifier 10.1109/TPEL.2023.3332641

I. Introduction

ENERGY consumption is an ever-growing demand worldwide because of the rising population, urbanization, and industrialization. Depletion of fossil fuels and penetration of renewable energy globally cause solar energy to be the optimum source of clean energy owing to its availability in abundance, sustainability, carbon emission free nature of operation, pollution free, noise-free, and eco-friendly. Recent developments in power electronics and photovoltaic (PV) cell technologies improved stability and efficiency under changing weather conditions. Among the power conversion topologies, the boost converter-based PV system has applications in dc microgrids based on PV, charging stations for electric vehicles, battery charging, rural electrification (PV powered lighting systems), and agriculture sector (PV water pumping applications) [1], [2], [3], [4], [5], [6]. It is required to develop an efficient control algorithm for extraction of the maximum power of a PV cell from very highly nonlinear $I-V$ and $P-V$ characteristics with irradiance and temperature variations by regulating the operating point.

Various maximum power point tracking (MPPT) control algorithms have been proposed [7], [8] to obtain the MPP of a PV system. The commonly used algorithm is perturb and observe (P&O), incremental conductance, short-circuit current, and open-circuit voltage algorithms [9], [10]. The primary drawbacks of these systems are their inconsistent response under variable load power and load current, which affect the system efficiency and power quality. Recently optimization methods have been proposed like genetic algorithm (GA), particle swarm optimization (PSO), gray wolf optimization (GWO), and ant colony optimization (ACO) [11], [12], [13] in addition to the above MPPT algorithms for ensuring a high probability of reaching the MPP, but still suffers from convergence problems [14]. In [4], an artificial neural network (ANN) is used to detect the region containing the global MPP, and the P&O algorithm is introduced to find the optimum point of the maximum power extraction. Fuzzy logic-based control [15] methods are characterized by their fast response time to reach the MPP. These methods reduce the system efficiency due to the convergence and are characterized by their implementation complexity [14]. To overcome the disadvantages of the aforementioned MPPT

algorithms, a robust functional expanded multikernel broad learning system (RFEMBLS) is proposed in the PV battery dc microgrid system.

A number of linear control schemes have been proposed to control the dc bus voltage. These schemes ignore the nonlinear nature of the dc–dc converters. Droop control, adaptive droop control, and proportional integral (PI) control are the most commonly used algorithms for regulating the dc bus voltage [11], [12], [13]. Due to the intermittent behavior of renewable energy sources (RES), fuzzy-based H-infinity control method and fuzzy-based exponential stability control method are not explored in [13]. When loads fluctuate quickly, generation ceases abruptly, etc., these control methods fail for the dc microgrid. Due to its fast dynamics and simplicity, conventional control methods like sliding mode control (SMC) are effective and resilient nonlinear controllers [16], [17], [18], [19]. When there is no energy storage technology that can provide quick response for increasing load requirements, SMC is employed in [16] to sustain the dc bus voltage fluctuations. This strategy is not appropriate because it is sensitive to outside disturbances and has chattering problems. Back stepping control is used for a wind system [20] and the chattering problem arises during control while sharing the power with multiple RES. Adaptive backstepping is investigated for an independent dc microgrid with one PV unit, but not discussed only for PV MPPT in [21]. In [22], the authors explored integral backstepping control for dc microgrids with multiple RES. This controller is more robust, but has chattering and steady-state inaccuracies. SMC with an integral backstepping controller for a PV considered in [23]. Another integral action term is added to the sliding surface as double integral [24] to reduce the steady-state error. The controller has achieved greater steady-state error minimization and at the same time, the amount of overshoot increased significantly. An adaptive integral derivative sliding mode controller is proposed [25] to eliminate the overshoot and minimize the steady-state fluctuation and verified by using the hardware in loop.

In [26], Chua's uncertain switching system is discussed using an adaptive composite nonlinear feedback integral sliding mode tracker architecture. This approach guarantees resistance to the effects of uncertainty and input saturation while also reducing chattering. Roy et al. [27] depicted a grid tied solar PV unit with a robust backstepping integral terminal sliding mode controller (TSMC). The design of a sliding mode MPPT controller [28] uses neural networks for standalone PV systems, and this control technique eliminates reaching phase, resulting in a continuous sliding mode. There are no harmonic distortions or chatter in the system response. Fuzzy recurrent neural control of a nonlinear system is introduced [29] by a terminal sliding mode controller, and the addition of the outer layer feedback improves the capability of dynamic approximation. In [30], for finite time reference signal tracking, a terminal SMC of the integral type is designed. Meanwhile, the proposed TSMC uses a saturation function to address the chattering problem under consideration. A combination of a SMC and a linear extended state observer is presented [31]. This method reduces sliding surface chattering and enhances performance in the face of abrupt static and dynamic load fluctuations as well as voltage changes at the input of the power supply.

To overcome the drawbacks of the control schemes stated above, a new decentralized control is proposed using an integral backstepping and SMC along with adaptiveness. The adaptive feature can minimize the system parameter variations. The SMC increases control accuracy and robustness of the system. The integral term enhances the tracking error convergence and reduces the steady-state error. The backstepping approach is utilized for fast response based on the feedback taken from the dc bus. The proposed work's main contributions are listed as follows.

1) A robust functional expanded multikernel broad learning system is proposed to compute the complex nonlinear maximum power point regression output more accurately for the PV distributed generation (DG) system by importing the functional expansion of the PV cell irradiance and temperature with less runtime.
2) An adaptive integral backstepping sliding mode controller is designed in this work to control the dc bus voltage of the proposed dc microgrid under abnormal scenarios. It ensures the entire dc microgrid remains stable despite load fluctuations, the unpredictable nature of RES, and external disturbances.
3) A PV system, a battery storage unit, and loads are integrated to build the dc microgrid. The main control task is to maintain a constant voltage on the dc bus by controlling the controllers of the connected components except for loads. A decentralized approach is adopted by using local information without any communication under different critical situations.
4) An asymptotical stability analysis of the proposed AIBSMC algorithm is derived using Lyapunov theory in the developed PV battery dc microgrid.
5) A new adoption rule of the proposed AIBSMC control algorithm for estimation of both PV voltage reference and battery current reference. Integral action is added to improve both the steady-state error and tracking error convergence. The backstepping method based on the dc bus voltage feedback results in faster response and reduced chattering. To improve the control precision and robustness, a sliding mode controller is proposed. The advantages of the proposed controller are compared with state-of-the-art methods recently developed and showcased in Table I. The droop control mechanism is introduced to obtain reference current with respect to battery current in order to reduce the dependence of the different RESs.
6) Finally, the proposed control algorithm is verified with dSPACE hardware in a loop platform to prove the feasibility, practicability, robustness, and efficacy of the developed system in the real-time scenario.

The rest of this article is organized as follows. The RFEMBLS method is explained in Section II to compute the PV reference voltage by importing the functional expansion of the irradiance and temperature. The adaptive integral backstepping SMC algorithm stability verifications in PV and battery systems are discussed in Section III. The detailed simulation results of different cases are presented in Section IV and the Ecosense

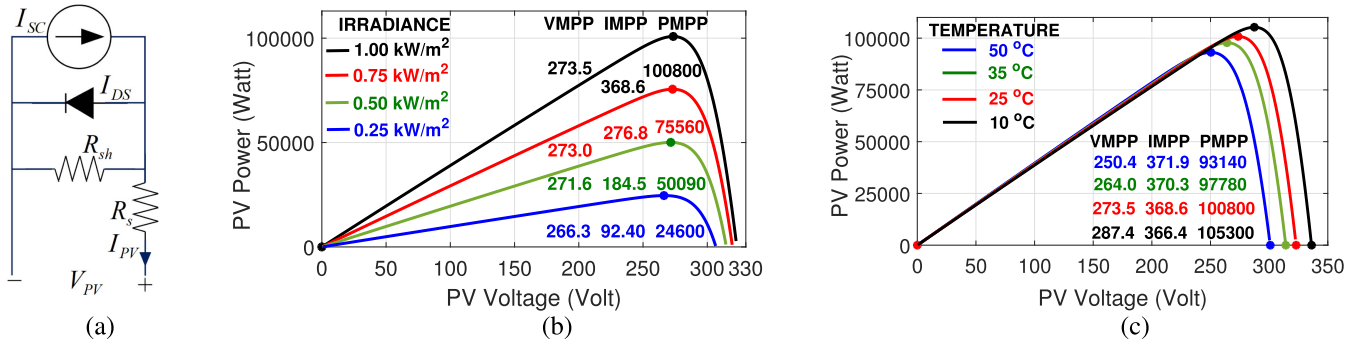

Fig. 1. $P-V$ module. (a) Internal structure using single diode. (b) Characteristics for different irradiation levels with fixed temperature at 25 °C Centigrade. (c) Characteristics for different temperature levels with fixed irradiation at 1000 W/m^2.

TABLE I
COMPARISON OF THE PROPOSED CONTROLLER WITH RECENTLY DEVELOPED PREVALENT METHODS

Ref	Control Method	Advantages	Disadvantages
[11-12]	Conventional	Highly reliable	Poor voltage regulation
[13]	H-infinity control	Robust control with minimum tracking error	Slow system response and dynamics
[16]	Sliding mode control	Robustness against large signal disturbances	Complexity in design and prone to chattering
[20]	Backstepping control	Global asymptotic stability and faster response	Low robustness against model uncertainties
[25]	Adaptive controller	Simple implementation and faster transient response	Slower adoption process
[26]	Adaptive composite nonlinear feedback integral SMC	Ensures resistance to the effects of uncertainty and input saturation while also reducing chattering	Low accuracy of reference tracking
[30]	Terminal SMC of the integral type	Uses a saturation function to address the chattering problem under consideration	Challenging computational burden
[31]	SMC with a linear extended state observer	Reduces sliding surface chattering and enhances performance under abrupt static and dynamic load fluctuations	No robustness against mismatched disturbances and chattering problem
This work	Adaptive integral backstepping SMC	The adaptive feature minimizes parameter variations, SMC improves control accuracy and robustness, the integral term enhances tracking error convergence and reduces steady state error, and the backstepping approach enables fast response using DC bus feedback	Complexity in the system

PV emulator with dSPACE1104 hardware test platform is used to validate the robustness of the proposed method in real time followed by the conclusion in Section V.

II. MPPT Modeling Based on Robust Functional Expanded Multikernel Broad Learning System

The PV cell is a p-n junction as presented in Fig. 1(a) and shows similar characteristics to a diode. PV voltage (V_{PV}) and current (I_{PV}) outputs are computed [32], [33] using the series resistance (R_s), shunt resistance (R_{sh}), light induced current (I_{sc}), p-n junction ideality factor (n), diode saturation current (I_{ds}), Boltzmann constant (K), electronic charge (q), junction temperature (T), temperature coefficient (h_t), and short-circuit current for reference irradiation (G_{ref}) with temperature (T_{ref}) as follows:

$$I_{sc} = I_{\text{ref}}\left[1 + h_t\left(T - T_{\text{ref}}\right)\right]\frac{G}{G_{\text{ref}}} \tag{1}$$

$$I_{\text{PV}} = I_{sc} - I_{ds}\left[\exp\left\{q(V_{\text{PV}} + I_{\text{PV}}R_s)/nKT\right\} - 1\right] - \left[(V_{\text{PV}} + I_{sc}R_s)/R_{sh}\right] \tag{2}$$

$$V_{\text{PV}} = \frac{nKT}{q}Ln\left(\frac{I_{sc}}{I_{\text{PV}}} + 1\right). \tag{3}$$

The Sunpower SPR-315E-WHT-D PV module is used to generate 100 kW power at 25°C temperature and 1000 W/m^2 irradiance by connecting 64 parallel strings with five different series arrays. The obtained maximum power (P_{MPP}) at maximum PV voltage (V_{MPP}) and current (I_{MPP}) for different temperatures as well as irradiances are presented in Fig. 1(b) and (c). It is necessary to develop a less computationally complex system to avoid issues such as inaccurate MPP values, output voltage fluctuations, steady-state oscillations, and large energy losses to compute V_{oc} or I_{sc}. This optimization is crucial for efficient PV system utilization under various operating conditions, including inconsistent irradiation, partial shading, load changes, and fault scenarios, often encountered in P&O, hill climbing, incremental conductance, constant voltage, and current tracking methods.

A simple, less computationally complex, easy implementable, and efficient versatile multikernel broad learning system is proposed. This system is based on very fast discriminative learning, better universal approximation, and fast remodeling without a retraining process to establish the complex nonlinear relationship more accurately. This is achieved by importing the functional expansion of the solar irradiance (G) and temperature (T) for obtaining the better regression performance of PV reference voltage (V_{PVref}) with less runtime. The exponential trigonometric expansion form of (G) and (T) of the PV module are $1, T, T^2, e^{-a|T|}\sin(\pi T), e^{-a|T|}\cos(\pi T)$, and $1, G, G^2, e^{-a|G|}\sin(\pi G), e^{-a|G|}\cos(\pi G)$, respectively. The functional expanded input data samples are first expanded into certain optimal nonadaptive random projection feature nodes and further transformed by multikernel function to obtain the

enhancement nodes. Both the feature and enhancement nodes update synchronously based on incremental learning and connect to the output layer for updating the flatted network structure dynamically. The kernel trick, as a new class of learning, is employed to compute the output weight matrix. This approach avoids the manual selection of enhancement nodes, random assignment of hidden node hyperparameters, and exhaustive parameter tuning, which are known to cause issues such as large training time, unstable model generalization, suboptimal network models, significant reconstruction errors, and increased computational overhead. The input dataset $X \in \Re^{n\times m}$ consists of n samples and each is equipped with m dimensions. The k number of feature mapping outputs (F) are computed by random assignment of weight (w_f) and bias (b_f) with activation function (Φ) as

$$(F_i)_{\text{RFEMBLS}} = \Phi \sum_{J=1}^{n} (w_{f_i} \cdot X_j + b_{f_i}); \quad i = 1, 2, \ldots, k. \tag{4}$$

The obtained feature nodes $F^k \equiv [F_1, F_2, \ldots, F_k]$ are further expanded as l enhancement nodes (E) by using random weight (w_e), bias (b_e), and activation function (Ψ) as follows:

$$(E_i)_{\text{RFEMBLS}} = \Psi \sum_{J=1}^{k} (w_{e_i} \cdot F_j + b_{e_i}); \quad i = 1, 2, \ldots, l. \tag{5}$$

The enhancement nodes $E^l \equiv [E_1, E_2, \ldots, E_l]$ with the feature nodes F^k are mapped to the output node (Y) to compute the output connecting weight matrix (β) as follows:

$$(\beta)_{\text{RFEMBLS}} = \left[F^k \mid E^l\right]^{\dagger} \cdot Y. \tag{6}$$

The input data samples are mapped directly to the output nodes to improve further the regression accuracy of the system. The output weight is computed as $(\beta)_{\text{RFEMBLS}} = [X^m \mid F^k \mid E^l]^{\dagger} \cdot Y$

$$= \begin{bmatrix} X^T \\ \overline{F^T} \\ \overline{E^T} \end{bmatrix} \left([X \mid F \mid E] \begin{bmatrix} X^T \\ \overline{F^T} \\ \overline{E^T} \end{bmatrix} + \frac{I}{\lambda} \right)^{-1} \cdot Y. \tag{7}$$

The multikernel function $\Omega_M = 0.3 \times \Omega_T + 0.7 \times \Omega_S$ as well as linear kernel (Ω_L) are introduced to develop RFEMBLS using tangent hyperbolic kernel (Ω_T) and sigmoid kernel (Ω_S). The output of RMKBLS $(f(\cdot))$ is computed by importing the input $[x^m \mid f^k \mid e^l]$ at testing stage as follows:

$$f_{(x^m|f^k|e^l)_{\text{RFEMBLS}}}$$

$$= [x \mid f \mid e] \begin{bmatrix} X^T \\ \overline{F^T} \\ \overline{E^T} \end{bmatrix} \left([X \mid F \mid E] \begin{bmatrix} X^T \\ \overline{F^T} \\ \overline{E^T} \end{bmatrix} + \frac{I}{\lambda} \right)^{-1} \cdot Y$$

$$= \left(xX^T + fF^T + eE^T\right) \left(XX^T + FF^T + EE^T + \frac{I}{\lambda} \right)^{-1}$$

$$\times Y = ([\Omega_M(x, X)] + [\Omega_M(f, F)] + [\Omega_M(e, E)])$$

$$\times \left([\Omega_L(X, X)] + [\Omega_L(F, F)] + [\Omega_L(E, E)] + \frac{I}{\lambda} \right)^{-1} \cdot Y. \tag{8}$$

III. Proposed AIBSMC Method

Conventional PI control algorithms [6], [7], [19] have been proposed to generate the reference signal. The integral and proportional gains in the PI control mechanism are denoted by the letters k_I and k_P [19]. The addition of integral action to a back stepping controller creates a nonlinear controller and is used in the dc microgrid system to reduce steady-state error and reach MPPT with lesser ripples as well as greater precision [1], [2], [3], [4] and [19], [20], [21]. Tracking the reference MPPT value of a PV network and lowering steady-state error are accomplished using a straightforward conventional sliding mode controller [4], [8]. In this work, an adaptive integral backstepping sliding mode control is proposed using the information based on both the integral backstepping and adaptive SMC algorithms. The developed controller consists of an inner nonlinear IBSMC loop to generate a control pulse for the PV boost converter and an outer MPPT control loop that provides a reference voltage to the earlier loop.

A. Boost Converter Control of PV System

The PV boost converter equations are defined as

$$\frac{dE_1}{dt} = \frac{(1 - S_{1p})E_2}{C_{\text{dc1}}} - \frac{E_1}{R_P C_{\text{dc1}}} \tag{9}$$

$$\frac{dE_2}{dt} = \frac{-(1 - S_{1p})E_1}{L_{\text{PV}}} - \frac{V_{\text{pv}}}{L_{\text{pv}}} \tag{10}$$

where E_1 is output voltage across C_{dc1}, E_2 is the PV converter current through L_{pv}, and S_{1p} is the control pulse for PV converter.

SMC, integral backstepping, and adaptive theory are integrated in the proposed control method for the PV converter system. Control pulse for the PV boost converter (S_{1p}) combines the SMC pulse $(S_{1\,s})$ and integral back stepping control pulse (S_1), i.e., $S_{1p} = S_1 + S_{1\,s}$.

1) Integral Back Stepping Control for PV System: The error (E_{R1}) based on the PV MPPT control reference voltage signal $(E_{1\text{ref}})$ of a PV converter [1], [4] is expressed as $(E_1 - E_{1\text{ref}})$. The derivative and integral term (E_p) of the error (E_{R1}) are considered to achieve zero convergence error. The first Lyapunov function (F_1) error must be zero and defined as $(\frac{1}{2}E_{R1}^2 + \frac{1}{2}q_1E_p^2)$. Time derivative, i.e., $(\dot{F}_1)$ should be negative to guarantee the system's asymptotic stability and the resultant expression is $(-q_2E_p^2)$, where q_1 and q_2 are positive definite real values. The capacitor output voltage reference is defined as

$$\lambda_1 = R_p C_{\text{dc1}} \left(\frac{(1 - s_1)E_2}{C_{\text{dc1}}} - \dot{E}_{1\text{ref}} + q_1E_p + q_2E_{R1} \right). \tag{11}$$

The capacitor voltage error E_{p1} is based on E_1 and MPPT reference λ_1 is $E_1 - \lambda_1$. The derivative of Lyapunov function (F_2) is equal to $\left(F_1 + \frac{1}{2}E_{p1}^2\right)$. It should be negative for global stability with the convergence of E_{R1} and E_{p1} to zero.

It is possible to stabilize PV system dynamics by equating the derivative of (F_2) to negative. $\dot{F}_2$ is computed using the aforementioned values as follows:

$$\dot{F}_2 = -q_2 E_{R1}^2 - q_3 E_{p1}^2. \tag{12}$$

By using the above-mentioned equations and derivative of (11) in (12) to compute the derivative of PV converter duty cycle $\dot{S}_1$ as

$$\dot{S}_1 = \frac{-1}{R_p E_2}\left(\frac{(1-S_1)E_2}{C_{\text{dc1}}} - \frac{E_1}{R_P C_{\text{dc1}}} - R_P C_{\text{dc1}} \times \left(\frac{-(1-S_1)^2 E_1}{L_{\text{PV}} C_{\text{dc1}}} + \frac{V_{\text{pv}}(1-S_1)}{L_{\text{PV}} C_{\text{dc1}}} - \dot{E}_{1\text{ref}} + q_1 E_{R1} + q_2 \times \left(\frac{-E_{P1}}{R_P C_{\text{dc1}}} - q_2 E_{R1} - q_1 E_p\right)\right) - \frac{E_{R1}}{R_P C_{\text{dc1}}} + q_3 E_{p1}\right) \tag{13}$$

where q_3 denotes positive constant, $S_1 \in [0,1]$ and $R_p, E_2 \neq 0$. The desired value of integral backstepping control (S_1) is obtained by integrating (13). This integral backstepping control is a part of the control pulse for the PV boost converter, which is generated by the control law as shown in (13) and is determined by using Lyapunov stability theorem. As a result, the system guarantees asymptotic stability as well as zero dynamic error convergence.

2) PV System Adaptive Theory: The internal fluctuations of the PV system lead to adding nonlinearity [22] in the voltage and current. The adoption laws are proposed for the proper functioning of a PV system. The voltage and current tracking errors such as $\hat{E}_1$ and $\hat{E}_2$ are defined as $(E_1 - \tilde{E}_1)$ and $(E_2 - \tilde{E}_2)$, respectively. The estimated outputs of E_1 and E_2 are $\tilde{E}_1$ equal to V_{dc1ref} and $\tilde{E}_2$ equal to $\frac{V_{\text{dc1ref}}^2}{\tilde{V}_{\text{pv}} \cdot \tilde{R}_p}$, where V_{dc1ref} denotes the desired dc bus voltage. The $\tilde{V}_{\text{pv}}$ and $\tilde{R}_p$ are chosen as the estimation parameters due to the voltage and current fluctuations in the output capacitor are caused by variations in the internal and load resistances of the PV system. The observation equations based on actual and estimated values are defined by magnifying the error, i.e., $\gamma_1 > 0$ and $\gamma_2 > 0$ as

$$\dot{\hat{E}}_1 = \frac{(1-S_1)\hat{E}_2}{C_{dc1}} - \frac{S_1 \hat{G}_p}{C_{\text{dc1}}} - \gamma_1 \hat{E}_1 \tag{14}$$

$$\dot{\hat{E}}_2 = \frac{-(1-S_1)\hat{E}_1}{L_{\text{pv}}} + \frac{\hat{v}_{\text{pv}}}{L_{\text{pv}}} - \gamma_2 \hat{E}_2. \tag{15}$$

The adoption laws are built using the quadratic Lyapunov function with the design values $(\gamma_1, \gamma_2) > 0$, $\hat{G}_p = G_p - \tilde{G}_p$, $G_p = 1/R_p$ and presented as

$$F_3 = \frac{1}{2} C_{\text{dc1}} \hat{E}_1^{\,2} + \frac{1}{2} L_{\text{pv}} \hat{E}_2^{\,2} + \frac{1}{2\alpha_1} L_{\text{pv}} \hat{G}_p^{\,2} + \frac{1}{2\alpha_2} L_{\text{pv}} \hat{V}_{\text{pv}}^2. \tag{16}$$

3) SMC for PV System: A sliding surface $(S_{1\,s})$ is defined as $(\hat{E}_1 + \eta_1 \int \hat{E}_1)$ to make sure the system reaches the desired value [25], [34]. The discontinuous law is used for the reduction of ripples as well as chattering and expressed as S_{1n}, which is equal to $(-\eta_1 \text{Sgn}(S_{1\,s}))$. A modest positive number of sizeable constant (η_1) is chosen from numerous simulation and experiment results to maintain stability and reduce the effect of the chattering of the system. Also, S_{1s} is the summation of equivalent control law $(S_{1\text{eq}})$ and discontinuous control law S_{1n}. The proposed AIBSMC output (F_4) is finally obtained by adding S_1 to the integration of S_{1n} as S_1^2 with the derivative of $2S_1\dot{S}_1$. Furthermore, the final PV converter system control pulse (S_{1p}) using positive constant η_1 and $\hat{E}_2$ is calculated as

$$S_{1p} = \int \dot{S}_1 + 1 - \frac{(E_1 \hat{G}_p + \gamma_1 C_{\text{dc1}} \hat{E}_1 - \eta_1 \hat{E}_1)}{\hat{E}_2} - \eta_1 \text{Sgn}(S_{1\,s}). \tag{17}$$

The control pulse for the PV boost converter is produced by the control law described in (17), and this results in asymptotic stability as well as the error reaches to zero over finite time. The developed AIBSMC control for the PV network is represented by the Lyapunov function (F_{PV}) and expressed as $(F_2 + F_3 + F_4)$, where F_2, F_3, and F_4 are the Lyapunov functions for the integral backstepping part, adaptive part, and sliding mode part, respectively. Since all the parts are negative semidefinite, the PV network gains global stability. F_{PV} should be negative semidefinite to acquire asymptotic stability

$$\dot{F}_{PV} = -q_2 e_p^2 - q_3 e_{p1}^2 - \gamma_1 C_{\text{dc1}} \hat{E}_1^{\,2} - \gamma_2 L_{\text{pv}} \hat{E}_2^{\,2} - 2S_{1\,s}\eta_1 \times \text{Sgn}(S_{1\,s}). \tag{18}$$

The PV system acquires global stability using Lyapunov theory since all parts are negative and semidefinite.

B. Modeling of the Battery System

Buck–boost converter topology is used to link the battery with the dc bus. This topology consists of an inductor (L_b), two MOSFET devices (SW_2, SW_3) and dc bus capacitor (C_{dc2}) as shown in Fig. 2. MOSFET switches are controlled by the gate signal generated by pulsewidth modulation (PWM). In the proposed system interceptive approach is used to generate a PWM signal. Due to the PWM control of the frequency, any switching noise that arises may be anticipated, simplifying the filtering procedure. The output capacitor acts as a filter in the circuit. Depending upon the load variation, the converter switches between boost mode and buck mode. When SW_2 is ON and SW_3 is OFF, the converter works as a boost circuit and the battery delivers to the dc bus $(I_{\text{bref}} > 0)$. Also, if SW_2 is OFF and SW_3 ON, the converter operates as a buck circuit and the battery draws power from the source $(I_{\text{bref}} < 0)$. Binary values such as 1 and 0 are used to describe the battery conditions in terms of the reference value of battery currents $(I_{\text{bref}} > 0$ & $I_{\text{bref}} < 0)$, respectively. The battery converter equations for $(I_{\text{bref}} > 0)$ are defined as

$$\frac{dI_b}{dt} = \frac{V_b}{L_b} - \frac{(1-S_2)V_{\text{dc}b}}{L_b} \tag{19}$$

$$\frac{dV_{\text{dc2}}}{dt} = \frac{(1-S_2)I_b}{C_{\text{dc2}}} - \frac{V_{\text{dc}b}}{R_b C_{\text{dc2}}} \tag{20}$$

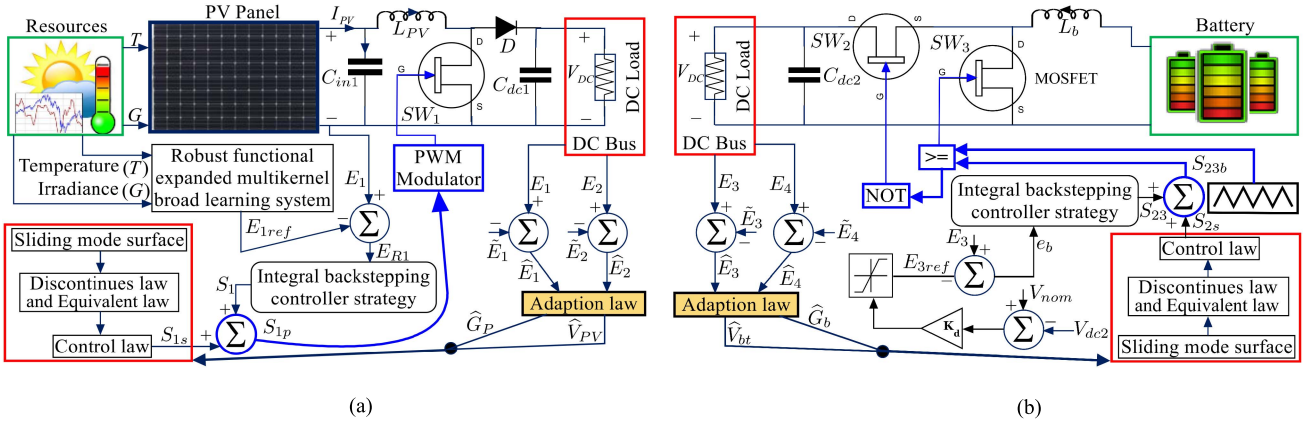

Fig. 2. Block diagram representation of the proposed RFEMBLS-AIBSMC method in (a) PV system and (b) battery system of DC microgrid.

where V_b is voltage across battery and $V_{\mathrm{dc}b}$ is voltage across battery converter. During $(I_{b\mathrm{ref}} < 0)$:

$$\frac{dI_b}{dt} = \frac{V_b}{L_b} - \frac{S_3 V_{\mathrm{dc}2}}{L_b} \tag{21}$$

$$\frac{dV_{\mathrm{dc}2}}{dt} = \frac{S_3 I_b}{C_{\mathrm{dc}2}} - \frac{V_{\mathrm{dc}b}}{R_b C_{\mathrm{dc}2}}. \tag{22}$$

The virtual control law is initialized to make a simpler system and depicted as follows:

$$S_{23b} = [\delta(1 - S_2) + (1 - \delta)S_3]. \tag{23}$$

By using (23), the simplified battery equations are as follows:

$$\frac{dE_3}{dt} = \frac{V_b}{L_b} - \frac{S_{23b}E_4}{L_b} \tag{24}$$

$$\frac{dE_4}{dt} = \frac{S_{23b}E_3}{C_{\mathrm{dc}2}} - \frac{E_4}{R_b C_{\mathrm{dc}2}} \tag{25}$$

where E_3 is battery converter current I_b, E_4 is output battery converter voltage $V_{\mathrm{dc}2}$, S_{23b} is control pulse, and R_b is the load resistance of the battery.

1) Droop Control for Battery Energy Storage System: To stabilize the dc bus voltage $(V_{\mathrm{dc}2})$, the bidirectional buck–boost converter topology is used in the battery control scheme. Because of the nonminimum phase aspect of the buck–boost converter, dc bus nominal voltage (V_{nom}) is incapable of controlling the V_{DC} [3], [6]. The reference current of the battery $(I_{b\mathrm{ref}})$ is tracking by battery current (I_b) using droop control approach [14] to regulate $V_{\mathrm{dc}2}$ to V_{nom}. Current control and voltage control loops are considered for battery control. The current control adopts the proposed AIBSMC algorithm, and the voltage control at the outer loop utilizes a droop operation. The voltage droop operation uses the voltage error acquired from V_{nom} and $V_{\mathrm{dc}2}$ to provide a current reference of the battery, which is further fed to the inner loop current control. In $(V_{\mathrm{dc}2} > V_{\mathrm{nom}})$ for starting the current control loop, the droop control yields a negative current reference. Because of this, current flows from the dc link to the battery, resulting in a battery charging scenario. A positive magnitude of the current reference for $(V_{\mathrm{dc}2} < V_{\mathrm{nom}})$ provides the power to the dc link and battery discharges. The formulation to compute the reference current using droop coefficient (K_d) is written as follows:

$$I_{b\mathrm{ref}} = -K_d(V_{\mathrm{nom}} - V_{\mathrm{dc}2}). \tag{26}$$

2) Integral Back Stepping Control for Battery System: The SMC pulse $(S_{2\,s})$ and integral backstepping control pulse (S_{23}) are integrated to form the battery converter control pulse (S_{23b}). The current error (e_b) of the battery converter $(E_3 - E_{3\mathrm{ref}})$ should converge to zero with its integral term (ϵ_b) to achieve the objective, where $E_{3\mathrm{ref}}$ is the reference current signal acquired from the droop control. It is believed that the first Lyapunov function has an error of zero

$$F_5 = \frac{1}{2}e_b^2 + \frac{1}{2}q_4\epsilon_b^2 \tag{27}$$

where q_4 is the asymptotically useful positive real value that is important for the system's stability. The time derivative of the Lyapunov function should be less than zero to guarantee stability. The derivative form of F_5 is defined using a positive constant q_5 as $(-q_5 e_b^2)$. The reference voltage across the output capacitor is defined as

$$\lambda_2 = \frac{L_b}{S_{23}}\left(\frac{V_{bt}}{L_b} - \dot{E}_{3\mathrm{ref}} + q_4\epsilon_b + q_5 e_b\right). \tag{28}$$

The error voltage (e_{b1}) across the capacitor is $(E_4 - \lambda_2)$ and should be zero to ensure that voltage across the output capacitor converges to the reference voltage generated from MPPT (λ_2). The derivative of the second Lyapunov function (F_6) must be negative to achieve global stability with the convergence of e_b and e_{b1} to zero

$$F_6 = F_5 + \frac{1}{2}e_{b1}^2 \tag{29}$$

$$\dot{S}_{23} = \frac{S_{23}}{\lambda_2}\left(\frac{-S_{23}E_3}{c_{\mathrm{dc}2}} + \frac{E_4}{R_b C_{dc2} + \frac{e_b S_{23}}{L_b}} - \frac{L_b q_5^2 q_4 \epsilon_b}{S_{23}} - q_6 e_{b1} + \frac{\dot{v}_{bt}}{S_{23}} - \frac{L_b \ddot{E}_{3\mathrm{ref}}}{S_{23}} - \frac{L_b q_4 e_b}{S_{23}}\right). \tag{30}$$

The required pulse for the battery converter (S_{23}) is obtained through the integration of (30). The Lyapunov theorem is implemented to determine the duty cycle value of the battery converter network. As a result, the system consistently guarantees global stability.

3) Battery System Adaptive Theory: The necessary adoption laws are proposed for the battery system for safe functioning and continuous current control as the internal variations frequently add nonlinear properties [21], [34] to output capacitor voltage and inductor current. The tracking errors of current (E_3) and voltage (E_4) are defined as ($E_3 - \tilde{E}_3$) and ($E_4 - \tilde{E}_4$), respectively, where the estimation of E_3 and E_4 are $\tilde{E}_3$ and $\tilde{E}_4$. Usually, $\tilde{E}_3$ equals to ($V_{\text{dc2ref}}^2/\tilde{V}_{bt}\tilde{R}_b$) and $E_4 = V_{\text{dc2ref}}$. Here, V_{dc2ref} indicates the desired dc bus voltage. Variations in output capacitor voltage and inductor current are caused by variations in battery internal and load resistances. Therefore, $\tilde{V}_{bt}$ and $\tilde{R}_b$ are chosen as the estimation parameters. The observation equations are written using estimation parameters $\tilde{V}_{bt}$ and $\tilde{R}_b$ with positive integer values γ_3 and γ_4 as

$$\dot{\tilde{E}}_3 = \frac{-S_{23}\tilde{E}_4}{L_b} + \frac{\tilde{V}_{bt}}{L_b} - \gamma_3\hat{E}_3 \tag{31}$$

$$\dot{\tilde{E}}_4 = \frac{-S_{23}\tilde{E}_3}{c_{dc2}} + \frac{R_b C_{dc2}}{L_b} - \gamma_4\hat{E}_4. \tag{32}$$

The derivative form of the Lyapunov function by using two positive values γ_3 and γ_4 with $G_b = 1/R_b$ is written as

$$\dot{F}_7 = L_b\hat{E}_3\dot{\tilde{E}}_3 + C_{\text{dc2}}\hat{E}_4\dot{\tilde{E}}_4 + \frac{1}{\alpha_3}\hat{G}_b\dot{\tilde{G}}_b + \frac{1}{\alpha_4}\hat{V}_{bt}\dot{\tilde{V}}_{bt}. \tag{33}$$

4) SMC for Battery System: A sliding surface ($S_{2\,s}$) is defined as ($S_{2seq} + S_{2sn}$) for the battery buck–boost converter system to make sure the system reaches the desired value [25], [34]. The proposed AIBSMC output (F_8) is computed as

$$\dot{F}_8 = -2S_{2\,s}\eta_2\text{Sgn}(S_{2\,s}). \tag{34}$$

The battery converter control pulse (S_{23b}) is expressed using positive constants γ_5, η_2, and ($\hat{E}_4 > 0$) as

$$S_{23b} = \int \dot{S_{23}} - \left(\frac{\gamma_5\hat{E}_3 L_b - \hat{V}_{bt} - \eta_2\hat{E}_3 L_b}{\hat{E}_4}\right) - \eta_2\text{sgn}(S_3). \tag{35}$$

The Lyapunov function (F_{Bat}) for the proposed AIBSMC of the battery converter network is expressed as

$$F_{\text{Bat}} = F_6 + F_7 + F_8 \tag{36}$$

where F_6, F_7, and F_8 are Lyapunov functions of integral backstepping control, adaptive theory, and SMC, respectively. The derivative of F_{Bat} should be negative to obtain asymptotic stability of the battery system.

C. Stability of the Proposed Control Algorithm

The closed-loop system stability of the proposed dc PV battery microgrid using the Lyapunov function of PV (F_{PV}) and battery (F_{bat}) is measured using overall Lyapuvnov function (F_f) and defined as

$$F_f = F_{\text{pv}} + F_{\text{bat}} = F_2 + F_3 + F_4 + F_6 + F_7 + F_8. \tag{37}$$

The negative derivative of (F_f) proves the equilibrium state of the proposed system with asymptotic stability based on the Lyapunov stability theorem and is presented as

$$\begin{aligned}\dot{F}_f = & -q_2e_p^2 - q_3e_{p1}^2 - \gamma_1 C_{\text{dc1}}\hat{E}_1^{\,2} - \gamma_2 L_{\text{pv}}\hat{E}_2^{\,2} - 2S_{1\,s}\eta_1 \\ & \times \text{Sgn}(S_{1s}) - q_5e_b^2 - q_6e_{b1}^2 - \gamma_3 C_{\text{dc2}}\hat{E}_3^{\,2} - \gamma_4 L_b\hat{E}_4^{\,2} \\ & - 2S_{2s}\eta_2\text{Sgn}(S_{2s}).\end{aligned} \tag{38}$$

The overall stability of the proposed microgrid is proved from (38) as $\dot{F}_f \leq 0$ and all the terms are negative semidefinite in the proposed control method. The state trajectories of the control law ensure the sliding surface based on the system stability.

In the PV boost converter implementation, AIBSMC is developed with an unknown load resistance and an unknown external input voltage. The robustness of the system is improved by an adaptive control mechanism. The adaptive controller ensures that the closed-loop systems are asymptotically stable in sliding mode by designing with state estimators. The estimations for the input voltage and load resistance also reach their authentic levels [17]. The output voltage tracks the reference voltage despite PV generation change, fault, and load variation, according to simulation and experimental data. The output voltage steady-state error is also quite small. To develop the adaptation laws for $\hat{G}_p$ and $\hat{V}_{\text{pv}}$, the estimates of G_p and V_{pv}, an estimator is employed. It can be written as $\hat{G}_p \to \frac{1}{R_p}$ and $\hat{V}_{\text{pv}} \to V_{\text{pv}}$ asymptotically. E_1 converges to V_{dc1ref} for the estimate $\hat{E}_1$ by a nearly exponential rate of $\frac{\hat{G}_p}{C_{\text{dc1}}} \to \frac{1}{R_pC_{\text{dc1}}}$, where R_pC_{dc1} is the time constant of the system. The $\hat{E}_1$ and $\hat{E}_2$ must reach zero for convergence. To guarantee that the observer (14) and (15) have quicker dynamics, the estimator gains γ_1 and γ_2 should be chosen to be significantly larger than $\frac{1}{R_pC_{\text{dc1}}}$. The minimum load anticipated in this case, $R_{p\text{min}}$, is assumed to be known. It is possible to use $\gamma_1 = \gamma_2 = \frac{5}{R_{p\text{min}}C_{\text{dc1}}}$ as the estimator gains initial value. Simulated results are used to determine the adaptation values and the initial factors.

IV. Simulation Results and dSPACE Hardware in Loop Verification

The effectiveness of the proposed control strategy of the PV battery dc microgrid as shown in Fig. 2 is simulated using MATLAB/Simulink software environment and verified in the dSPACE embedded processor by integrating the PV emulator. Several uncertainties like generation change, pole to pole dc side fault, and load variation are considered to validate the robustness of the proposed RFEMBLS-AIBSMC method as compared with existing algorithms based on chattering and steady-state time. The main objective of the proposed controller is to maintain voltage across the dc microgrid and the stability of the PV battery dc microgrid. The dc bus reference voltage is considered as 500 V and the simulation running time is considered as 5 s. The detailed specifications of the proposed dc microgrid are presented in Table II.

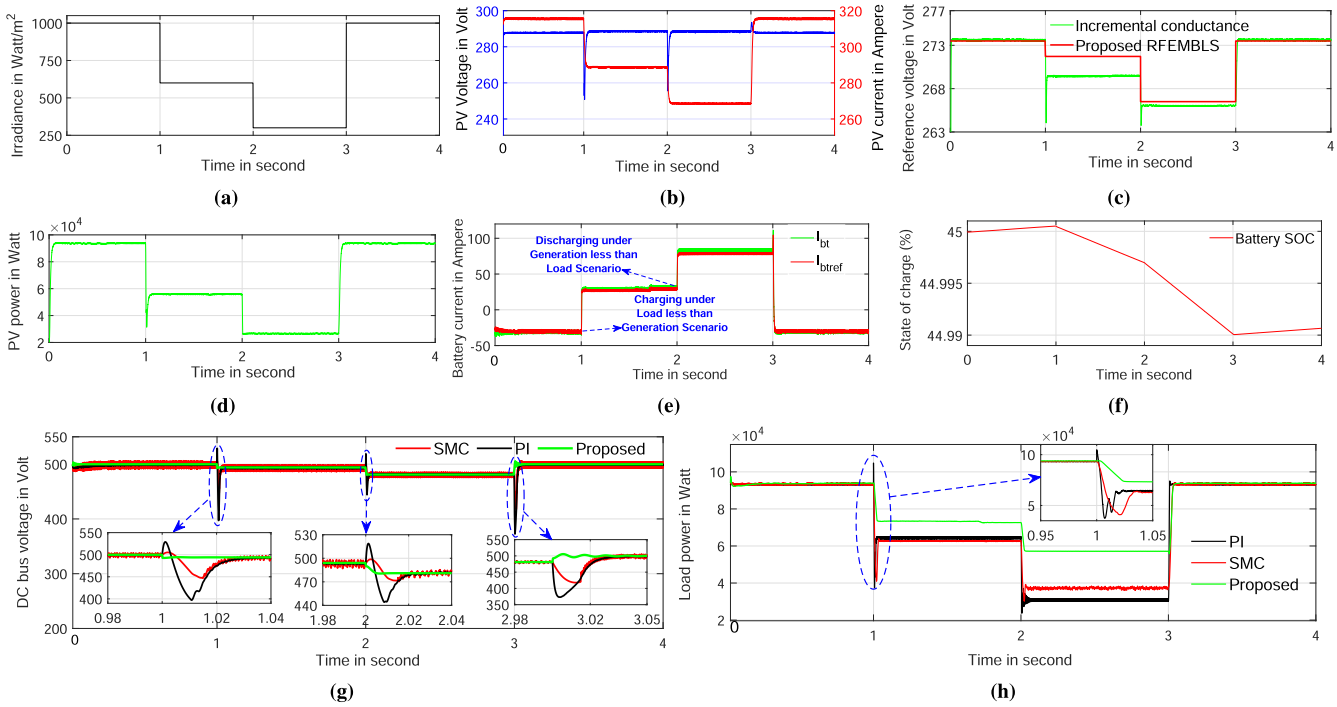

Fig. 3. Generation change results using RFEMBLS method. (a) Irradiance. (b) PV voltage and current. (c) PV reference voltage. (d) PV power. (e) Battery current. (f) Battery SOC. (g) DC bus voltage. (h) Load power.

TABLE II
DEVELOPED PV-BATTERY MICROGRID SPECIFICATIONS

PV boost converter specification		**Lithium battery system specification**	
Specification	**Ratings**	**Parameters**	**Ratings**
V_{OC}	322 V	Voltage	300 V
I_{SC}	394 A	Rated capacity	420 Ah
V_{MPP}	273.5 V	Nominal discharge current	174.912 A
I_{MPP}	368.6 A	Inductor	3.5 mH
Maximum power	100 kW	Output capacitance	3200 μF
Inductor	4 mH	**Proposed control parameters**	
Input capacitance	80 μF	**Parameters**	**Ratings**
Output capacitance	3200 μF	q_1, q_2, q_3	150, 80, 1100
Switching frequency	10 kHz	q_4, q_5, q_6	120, 1100, 3000

A. Case 1: Generation Change

In this scenario, the PV system is operated by varying irradiance and keeping the temperature constant at 25 °C as presented in Fig. 3. Fig. 3(a) shows irradiance change with different time intervals and the corresponding PV current as well as voltage changed according to irradiance value as reflected in Fig. 3(b). The reference voltage of the PV system is computed using incremental conductance [7] and the proposed RFEMBLS method, and is shown in Fig. 3(c). The robust reference voltage prediction accuracy of the RFEMBLS method supplies the maximum power to the load and PV power is presented in Fig. 3(d). It is observed that if the irradiance decreases then the PV power is decreasing and vice versa. The battery charging from 0 to 1 s and discharging up to 3 s responses are described under PV penetration variation in Fig. 3(e) and (f). When the irradiance is decreased, the load is greater than the generation that defines the system in power deficit. During this time, battery meets the power required by tracking the current reference accurately with the traditional droop control method. At 3 s the irradiance is increased, i.e., generation greater than the load demand. During this time, the battery is consuming energy from the dc bus, which is depicted in Fig. 3(e). In addition to this, the battery state of charge (SOC) during this scenario is shown in Fig. 3(f). The dc bus voltage under this scenario is illustrated in Fig. 3(g). It is observed that the proposed AIBSMC controller reaches a steady value within 0.021 s by minimum chattering and comprises no overshoot when compared with existing controllers such as PI and SMC. During the time instants of 1, 2, and 3 s, the transients present in the system under the generation change condition. However, the proposed AIBSMC algorithm performs the dynamic outcome quicker as compared to the state-of-the-art PI and SMC algorithms. The load power contains oscillation during the PV penetration change as depicted in Fig. 3(h) and the proposed AIBSMC controller shows no overshoot, minimum chattering, and quick response as compared with other prevalent methods.

B. Case 2: Pole-to-Pole Fault

The PV penetration is considered as 1000 W/m^2 with the temperature of 25 °C. The dc pole-to-pole (PP) fault is shown at various times and the transient behavior is illustrated in Fig. 4. Fig. 4(a) shows irradiance in different time intervals and the corresponding PV current as well as voltage are changed based on the fault instant as reflected in Fig. 4(b). When the PV power

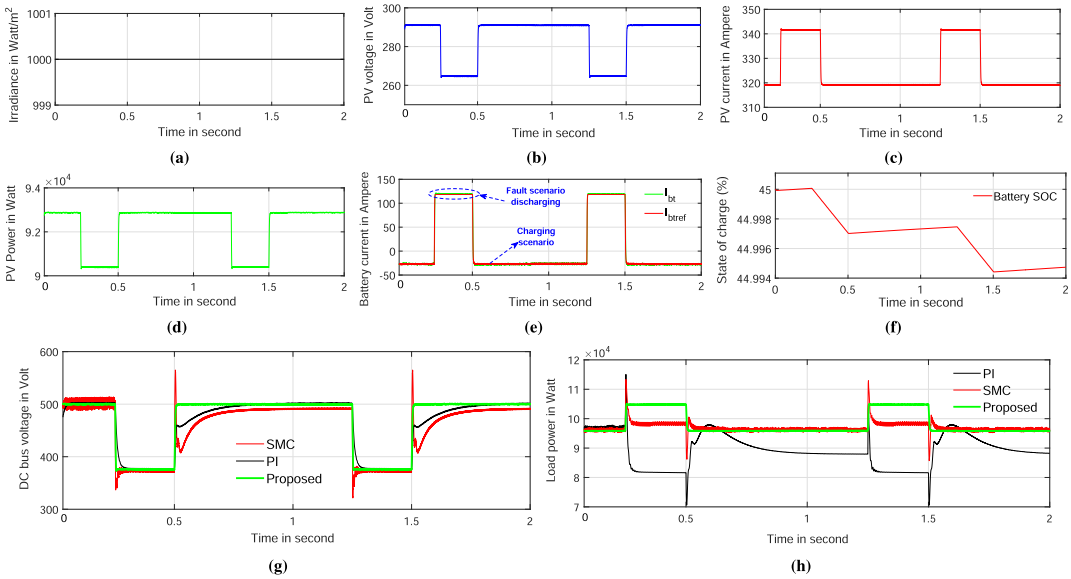

Fig. 4. DC PP fault results using RFEMBLS method. (a) Irradiance. (b) PV voltage. (c) PV current. (d) PV power. (e) Battery current. (f) Battery SOC, (g) DC bus voltage. (h) Load power.

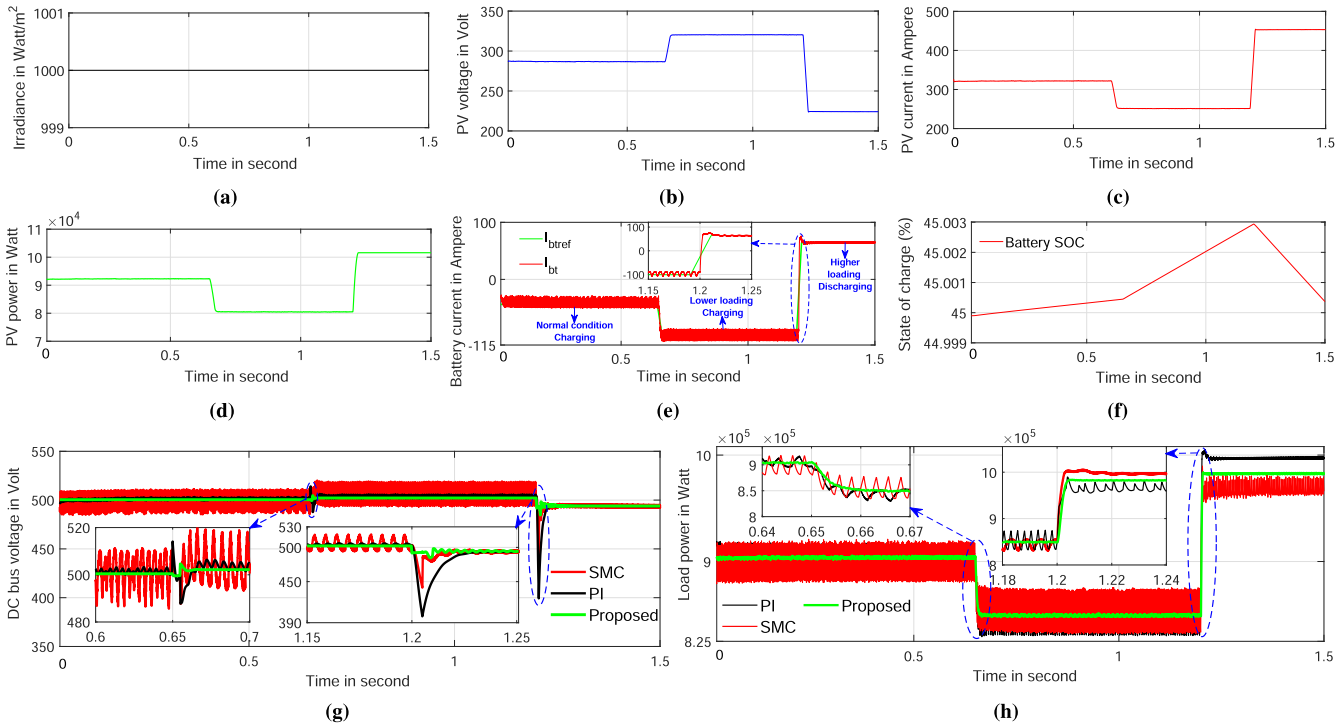

Fig. 5. DC load change results using RFEMBLS method. (a) Irradiance. (b) PV voltage. (c) PV current. (d) PV power. (e) Battery current. (f) Battery SOC. (g) DC bus voltage. (h) Load power.

decreases and subsequently, PV voltage drops, where the PV current rises significantly at the fault instant as shown in Fig. 4(c) and (d). Fig. 4(e) and (f) shows the battery response in the dc microgrid by the developed AIBSMC approach. It is obvious that the battery was charging before the issue because there is less load and more generation. According to Fig. 4(e), the battery accurately records positive reference current during fault instant from 0.25 to 0.5 s and 1.25 to 1.5 s. In this regard, the battery supplies a sudden power shortage. In addition, Fig. 4(f) presents a battery's SOC under a PP fault condition. Fig. 4(g) describes the voltage of the dc bus under the fault state and the transients occur at 0.25 and 1.25 s. The proposed AIBSMC

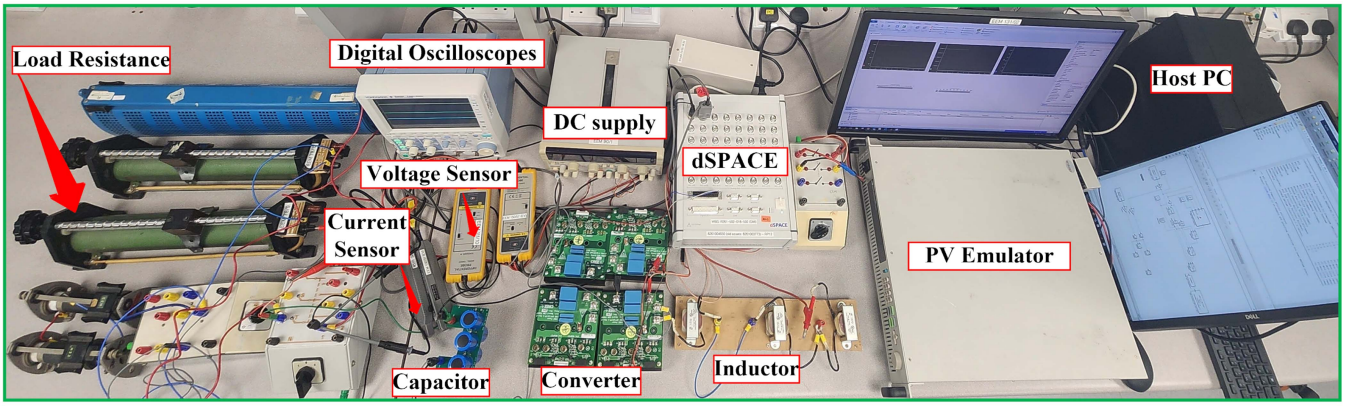

(a)

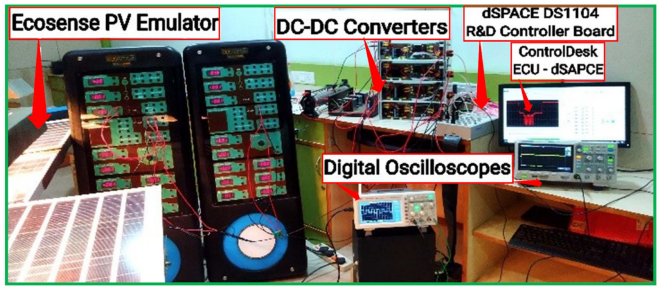

(b)

Fig. 6. (a) Detailed component label of hardware setup. (b) Overall test bench setup for the verification of proposed method in real time.

controller responds more quickly with no chattering as it was in existing controllers. The high current developed during a fault situation, and the corresponding power is depicted in Fig. 4(h). It is obvious that under a fault condition, the power transient's amplitude is very large. In contrast to existing methodologies, the proposed AIBSMC controller offers a smaller transient amplitude, a quicker dynamic response, and less chattering.

C. Case 3: DC Load Variation

In this case, PV irradiance and temperature are fixed at $1000\,\mathrm{W/m^2}$ and 25 °C, respectively, and represented in Fig. 5. The switching is considered from 0.5 to 1.5 s. In this regard, at 0.65 s lower dc loading, i.e., -25% and at 1.2 s higher loading, i.e., $+20\%$ loading occurred in the system. Fig. 5(a) is indicated at constant irradiance under dc load change. Subsequently, the changed voltage, current, and power of PV are also represented in Fig. 5(b) to (d). From this, it can be noticed that the PV power has been changed under lower and higher loadings. The performance of the battery by using the proposed controller is shown in Fig. 5(e) and (f). Further, the positive reference current of the battery is tracked under the discharge process, whereas the negative reference current of the battery is tracked during the charge process accurately. The battery SOC is depicted in Fig. 5(f) and the voltage across the dc bus is described in Fig. 5(g). From this, it is observed that the proposed AIBSMC controller reduces the transients under higher and lower loadings. Also, this controller has given a faster response with less chattering in comparison to PI and SMC controllers. Power across the load is depicted in Fig. 5(h). In Fig. 5(h), high transients are reduced by the proposed controller and it shows a quick response as compared to PI and SMC.

The cutting edge functionally expanded multikernel broad learning system significantly enhanced the accuracy of complex nonlinear maximum power point regression in PV DG systems. This advancement is achieved by leveraging functional expansion techniques to model PV cell irradiance and temperature dynamics, all while optimizing computational efficiency. A new adoption-based AIBSMC is capable of managing the dc bus voltage in our novel dc microgrid configuration, which integrates a PV system, battery storage unit, and diverse loads. This algorithm has integral action, resulting in substantial enhancements to both steady-state error minimization and tracking error convergence. Moreover, the backstepping control strategy based on dc bus voltage feedback ensures faster response times and mitigates control chatter. To improve the control precision and robustness, a sliding-mode controller is proposed. To minimize reliance on different RES, the droop control mechanism enables the determination of reference current relative to battery current, ultimately improving the overall efficiency of the system.

D. Experimental Verification of the Proposed Method Using Ecosense PV Emulator With dSPACE1104 R & D Board

The Ecosense PV plant prototype is connected with two ELODORA modules of 40 kW peak each as well as local loads of the developed dSPACE embedded processor based hardware in

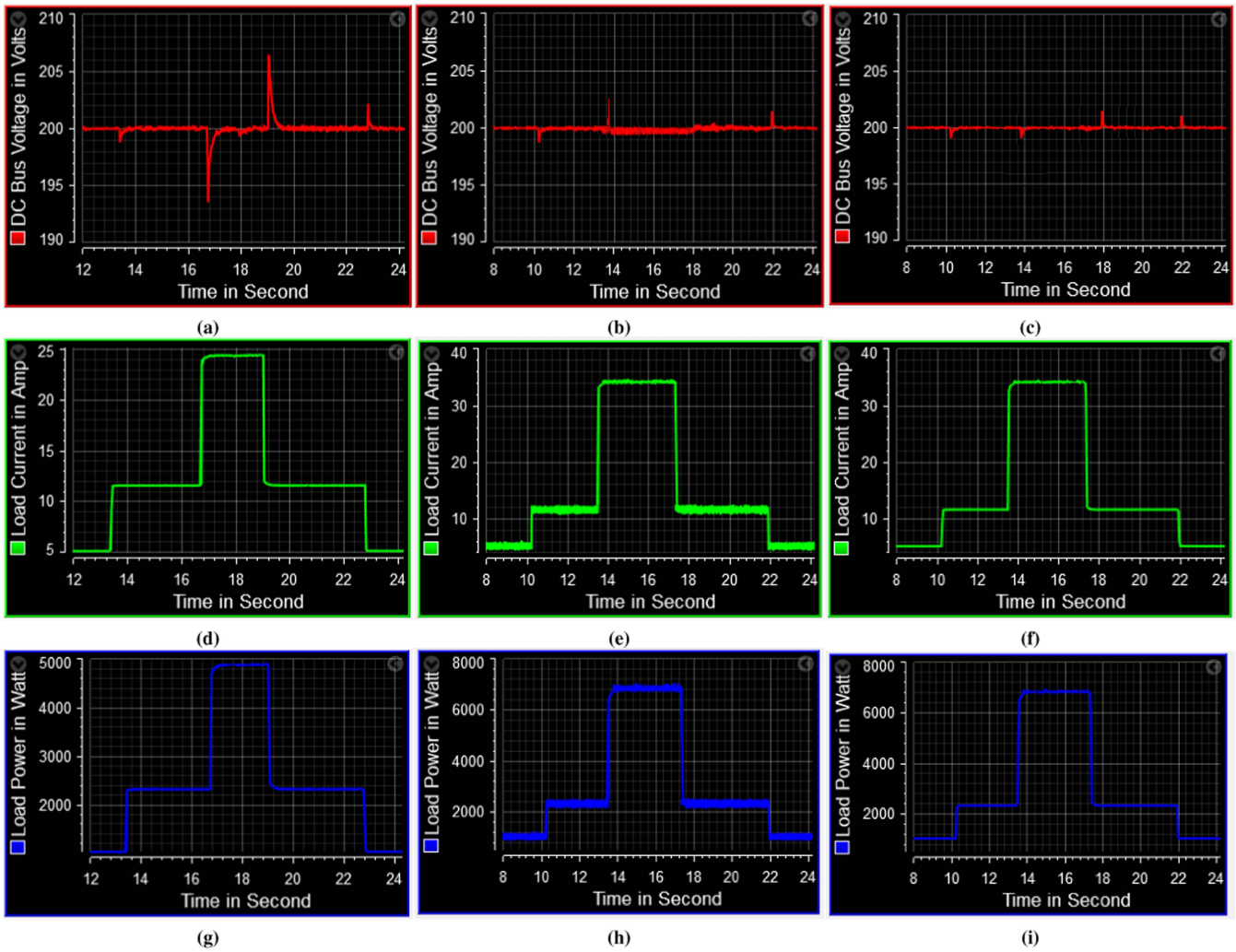

Fig. 7. Experimental verification using RFEMBLS method for dc load change condition. (a) DC bus voltage of PI. (b) DC bus voltage of SMC. (c) DC bus voltage of AIBSMC. (d) Load current of PI. (e) Load current of SMC. (f) Load current of AIBSMC. (g) Load power of PI. (h) Load power of SMC. (i) Load power of AIBSMC.

the loop (HIL) rapid controller prototyping model to validate the control strategy of the proposed RFEMBLS-AIBSMC method. Ecosense PV emulator consists of ELDORA-40 poly crystalline PV panels, 1.8-kW illumination controlled halogen bulbs artificial source for irradiation variation, and a variable RLC load up to 25 W with a provision for DG side faults to test and examines the proposed PV-battery-based dc microgrid. The 25-W dc–dc converter and 50-W dc–ac voltage source converter of the power conditioning unit (PCU) operate metal-oxide-semiconductor field effect transistor (MOSFET) based power switching. The PV emulator is interfaced with the dSPACE R&D control panel using Tektronix TPP0101 probe of 300 V peak with the operating frequency of 100 MHz. The embedded analog-to-digital converter (ADC) and digital-to-analog converter (DAC) channels operate with 10-kHz frequency of a maximum 250 MHz supporting operate value. Host PC based control desk software platform is used to operate the control logic of dc–dc voltage boost (VB) in the MATLAB/Simulink configured with dSPACE real-time interfacing (RTI) library with the supporting package. The master power PC $602e$ based DS1104 embedded processor records the PV voltage and current from the ADC ports through LEM 25 V and LEM $25P$ Ecosense sensors. The switching pulse of the proposed controller output as the duty cycle is fed to DAC through the TP0101 cable of dc–dc VB in an Ecosense PCU.

In our experimental setup at the Ecosense laboratory based on the dSPACE embedded processor, we created various scenarios involving changes in dc load and pole-to-pole faults. The detailed component-level configuration of this setup is illustrated in Fig. 6(a), while the overall test bench is depicted in Fig. 6(b). The ADC port of the dSPACE embedded development board is interfaced with practical scale down signals, and the control desk software environment is configured to capture the proposed control output windowed signal. The irradiance from the $E1$ and $E2$ is set at $1000\,\mathrm{W/m^2}$ using an adjustable knob of 1.8-KW halogen bulb corresponding to dc load change and pole-to-pole fault conditions. To verify the impact of the control action of

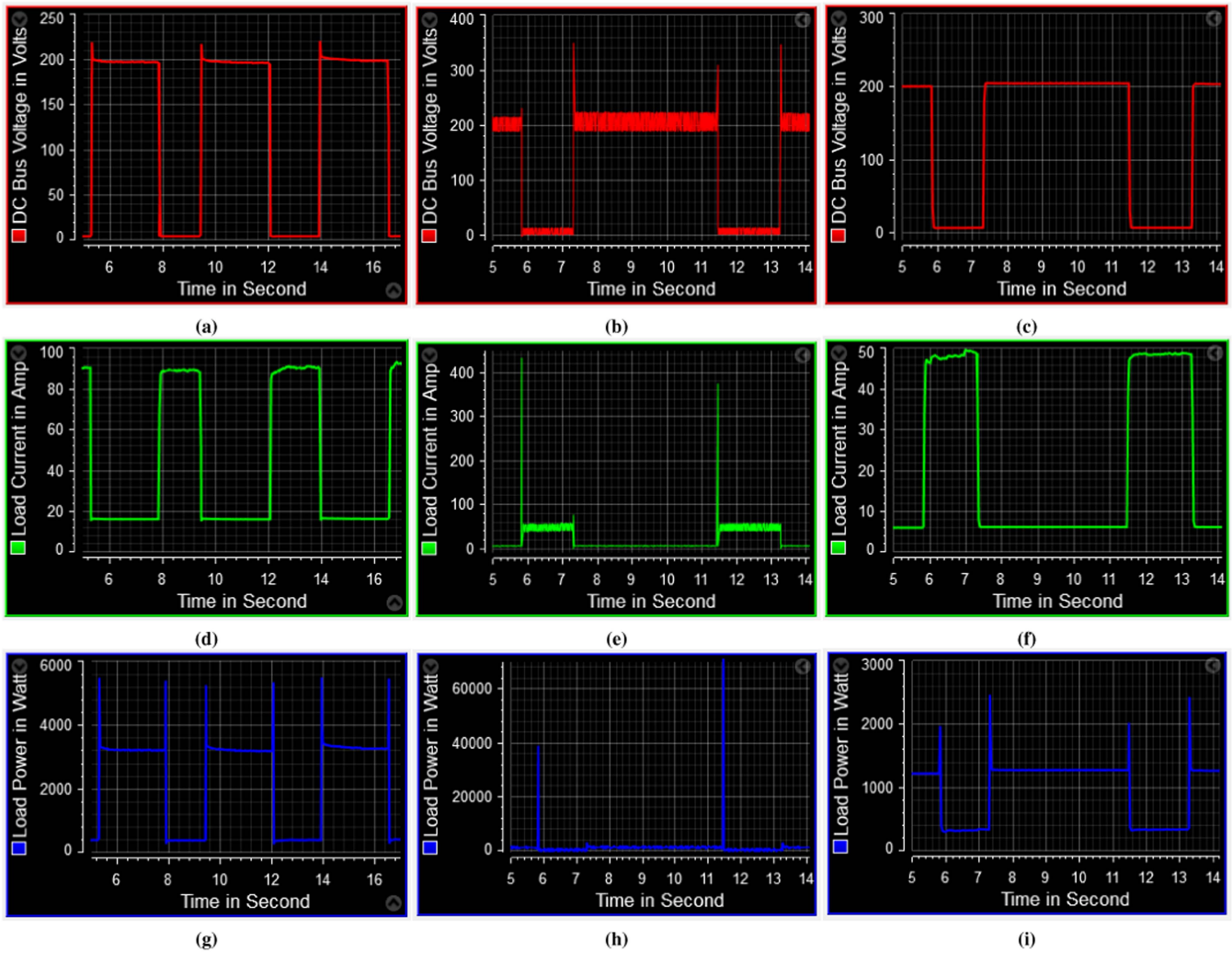

Fig. 8. Experimental verification based on RFEMBLS method for pole to pole fault condition. (a) DC bus voltage of PI. (b) DC bus voltage of SMC. (c) DC bus voltage of AIBSMC. (d) Load current of PI. (e) Load current of SMC. (f) Load current of AIBSMC. (g) Load power of PI. (h) Load power of SMC. (i) Load power of AIBSMC.

the proposed method, the dynamics of load change are initiated for $+10\%$ loading at 13.2 s, $+25\%$ loading at 16.8 s, -25% loading at 19.2 s, and -10% loading at 22.8 s. The recorded dc link voltage, load current, and load power outputs of the control desk environment under the dynamics of load change of RFEMBLS-PI, RFEMBLS-SMC, and RFEMBLS-AIBSMC control methods are presented in Fig. 7. From Fig. 7, it can be noticed that the proposed control shows less chatter with a higher response speed. Furthermore, a pole-to-pole fault is created with different switching times, and the recorded dc link voltage, load current, and load power outputs are presented in Fig. 8. From Fig. 8, it can be observed that the RFEMBLS-PI and RFEMBLS-SMC methods show more chattering and high oscillations. However, the RFEMBLS-AIBSMC proposed method shows less oscillations. Thus, the simulated and hardware results show the proposed controller maintains the dc bus voltage effectively under different scenarios as compared to other methods.

V. Conclusion

In this work, we have introduced the integration of a PV renewable energy source and the battery energy storage system with the dc bus. The outstanding reference value prediction efficacy of the proposed RFEMBLS method of the PV system is performed accurately by importing the functional expansion of the irradiance and temperature. The performance of the proposed approach is studied in terms of the dc bus voltage regulation as well as the transient responses of the states by using MATLAB/Simulink as well as experimentation to test it, and the outcomes are examined with PI and SMC. The proposed RFEMBLS-AIBSMC method shows excellent tracking results, quick steady-state error convergence, minimum chattering as well as ripples, and no overshoots over other recently developed prevalent control methods. Using the Lyapunov analysis, the system's overall asymptotic stability and zero dynamic error convergence have been verified. Finally, the simplicity,

practicability, and robustness of the proposed control algorithm are examined and validated in different scenarios in an Ecosense PV emulator interfaced with dSPACE1104 embedded processor.

REFERENCES

[1] S. H. Park, G. R. Cha, Y. C. Jung, and C. Y. Won, "Design and application for PV generation system using a soft-switching boost converter with SARC," *IEEE Trans. Ind. Electron.*, vol. 57, no. 2, pp. 515–522, Feb. 2010.

[2] M. Das and V. Agarwal, "Design and analysis of a high-efficiency DC–DC converter with soft switching capability for renewable energy applications requiring high voltage gain," *IEEE Trans. Ind. Electron.*, vol. 63, no. 5, pp. 2936–2944, May 2016.

[3] Q. Chen, N. Liu, C. Hu, L. Wang, and J. Zhang, "Autonomous energy management strategy for solid-state transformer to integrate PV-assisted EV charging station participating in ancillary service," *IEEE Trans. Ind. Inform.*, vol. 13, no. 1, pp. 258–269, Feb. 2017.

[4] Y. Hu, C. Gan, W. Cao, Y. Fang, S. J. Finney, and J. Wu, "Solar PV-powered SRM drive for EVs with flexible energy control functions," *IEEE Trans. Ind. Appl.*, vol. 52, no. 4, pp. 3357–3366, Jul./Aug. 2016.

[5] T.-F. Wu, C.-H. Chang, and Y.-H. Chen, "A fuzzy-logic-controlled single-stage converter for PV-powered lighting system applications," *IEEE Trans. Ind. Electron.*, vol. 47, no. 2, pp. 287–296, Apr. 2000.

[6] N. Priyadarshi, M. S. Bhaskar, S. Padmanaban, F. Blaabjerg, and F. Azam, "New CUK–SEPIC converter based photovoltaic power system with hybrid GSA–PSO algorithm employing MPPT for water pumping applications," *IET Power Electron.*, vol. 13, no. 13, pp. 2824–2830, 2020.

[7] B. Subudhi and R. Pradhan, "A comparative study on maximum power point tracking techniques for photovoltaic power systems," *IEEE Trans. Sustain. Energy*, vol. 4, no. 1, pp. 89–98, Jan. 2013.

[8] P. Joshi and S. Arora, "Maximum power point tracking methodologies for solar PV systems–a review," *Renewable Sustain. Energy Rev.*, vol. 70, pp. 1154–1177, 2017.

[9] V. Nayanar, N. Kumaresan, and N. A. Gounden, "A single-sensor-based MPPT controller for wind-driven induction generators supplying DC microgrid," *IEEE Trans. Power Electron.*, vol. 31, no. 2, pp. 1161–1172, Feb. 2016.

[10] M. R. Singaravel and S. A. Daniel, "MPPT with single DC–DC converter and inverter for grid-connected hybrid wind-driven PMSG–PV system," *IEEE Trans. Ind. Electron.*, vol. 62, no. 8, pp. 4849–4857, Aug. 2015.

[11] R. Sedaghati and M. R. Shakarami, "A novel control strategy and power management of hybrid PV/FC/SC/battery renewable power system-based grid-connected microgrid," *Sustain. Cities Soc.*, vol. 44, pp. 830–843, 2019.

[12] J. Hu, Y. Shan, Y. Xu, and J. M. Guerrero, "A coordinated control of hybrid AC/DC microgrids with PV-wind-battery under variable generation and load conditions," *Int. J. Elect. Power Energy Syst.*, vol. 104, pp. 583–592, 2019.

[13] P. Satapathy, S. Dhar, and P. K. Dash, "A new hybrid firefly optimized P-Q and V-f controller coordination for PV-DG–based microgrid stabilization," *Int. Trans. Elect. Energy Syst.*, vol. 28, no. 7, 2018, Art. no. e2568.

[14] A. Mohapatra, B. Nayak, P. Das, and K. B. Mohanty, "A review on MPPT techniques of PV system under partial shading condition," *Renewable Sustain. Energy Rev.*, vol. 80, pp. 854–867, 2017.

[15] P. Verma, R. Garg, and P. Mahajan, "Asymmetrical interval type-2 fuzzy logic control based MPPT tuning for PV system under partial shading condition," *ISA Trans.*, vol. 100, pp. 251–263, 2020.

[16] H. R. Baghaee, M. Mirsalim, G. B. Gharehpetian, and H. A. Talebi, "Decentralized sliding mode control of WG/PV/FC microgrids under unbalanced and nonlinear load conditions for ON-and OFF-grid modes," *IEEE Syst. J.*, vol. 12, no. 4, pp. 3108–3119, Dec. 2018.

[17] S. Oucheriah and L. Guo, "PWM-based adaptive sliding-mode control for boost DC–DC converters," *IEEE Trans. Ind. Electron.*, vol. 60, no. 8, pp. 3291–3294, Aug. 2012.

[18] Y. Shan, J. Hu, Z. Li, and J. M. Guerrero, "A model predictive control for renewable energy based AC microgrids without any PID regulators," *IEEE Trans. Power Electron.*, vol. 33, no. 11, pp. 9122–9126, Nov. 2018.

[19] S. Dhar and P. Dash, "A new backstepping finite time sliding mode control of grid connected PV system using multivariable dynamic VSC model," *Int. J. Elect. Power Energy Syst.*, vol. 82, pp. 314–330, 2016.

[20] H. Delavari and S. Naderian, "Backstepping fractional sliding mode voltage control of an islanded microgrid," *IET Gener. Transmiss. Distrib.*, vol. 13, no. 12, pp. 2464–2473, 2019.

[21] T. K. Roy, M. A. Mahmud, A. M. T. Oo, M. E. Haque, K. M. Muttaqi, and N. Mendis, "Nonlinear adaptive backstepping controller design for islanded DC microgrids," *IEEE Trans. Ind. Appl.*, vol. 54, no. 3, pp. 2857–2873, May/Jun. 2018.

[22] H. Armghan, M. Yang, M. Wang, N. Ali, and A. Armghan, "Nonlinear integral backstepping based control of a DC microgrid with renewable generation and energy storage systems," *Int. J. Elect. Power Energy Syst.*, vol. 117, 2020, Art. no. 105613.

[23] B. K. Oubbati, M. Boutoubat, A. Rabhi, and M. Belkheiri, "Experiential integral backstepping sliding mode controller to achieve the maximum power point of a PV system," *Control Eng. Pract.*, vol. 102, 2020, Art. no. 104570.

[24] J. Fei, H. Wang, and Y. Fang, "Novel neural network fractional-order sliding-mode control with application to active power filter," *IEEE Trans. Syst., Man, Cybern., Syst.*, vol. 52, no. 6, pp. 3508–3518, Jun. 2022.

[25] N. Bouarroudj, D. Boukhetala, B. Benlahbib, and B. Batoun, "Sliding mode control based on fractional order calculus for DC-DC converters," *Int. J. Math. Model. Comput.*, vol. 5, no. 4 pp. 319–333, 2015.

[26] S. Amiri, S. M. Seyed Moosavi, M. Forouzanfar, and E. Aghajari, "Adaptive composite nonlinear feedback integral sliding mode tracker design for Chua's uncertain switched system," *Int. J. Control*, pp. 1–10, 2022.

[27] C. Roy, T. K. Roy, and L. C. Paul, "Robust backstepping integral terminal sliding mode controller for a grid-tied solar PV unit," in *Proc. IEEE Int. Conf. Power Elect. Electron. Ind. Appl.*, 2021, pp. 37–40.

[28] I. U. Haq et al., "Neural network-based adaptive global sliding mode MPPT controller design for stand-alone photovoltaic systems," *PLoS One*, vol. 17, no. 1, 2022, Art. no. e0260480.

[29] J. Fei, Y. Chen, L. Liu, and Y. Fang, "Fuzzy multiple hidden layer recurrent neural control of nonlinear system using terminal sliding-mode controller," *IEEE Trans. Cybern.*, vol. 52, no. 9, pp. 9519–9534, Sep. 2022.

[30] S. Hou, Y. Chu, and J. Fei, "Adaptive type-2 fuzzy neural network inherited terminal sliding mode control for power quality improvement," *IEEE Trans. Ind. Inform.*, vol. 17, no. 11, pp. 7564–7574, Nov. 2021.

[31] J. Linares-Flores et al., "Sliding mode control based on linear extended state observer for DC-to-DC buck–boost power converter system with mismatched disturbances," *IEEE Trans. Ind. Appl.*, vol. 58, no. 1, pp. 940–950, Jan./Feb. 2022.

[32] N. Femia, G. Petrone, G. Spagnuolo, and M. Vitelli, "Optimization of perturb and observe maximum power point tracking method," *IEEE Trans. Power Electron.*, vol. 20, no. 4, pp. 963–973, Jul. 2005.

[33] S. Liu and R. A. Dougal, "Dynamic multiphysics model for solar array," *IEEE Trans. Energy Convers.*, vol. 17, no. 2, pp. 285–294, Jun. 2002.

[34] M. B. Delghavi, S. Shoja-Majidabad, and A. Yazdani, "Fractional-order sliding-mode control of islanded distributed energy resource systems," *IEEE Trans. Sustain. Energy*, vol. 7, no. 4, pp. 1482–1491, Oct. 2016.

Mrutyunjaya Sahani (Senior Member, IEEE) received the B.Tech. degree in electrical engineering from the Biju Patnaik University of Technology, Rourkela, India, in 2007, the M.Tech. degree in embedded system technology from the SRM University, Chennai, India, in 2010, and the Ph.D. degree in electronics and communication engineering from Siksha 'O' Anusandhan University, Odisha, India, in 2019.

He is currently a Research Fellow with the Department of Electrical and Computer Engineering, National University of Singapore, Singapore. His current research interests include power quality analysis, power system protection, signal processing, micro and smart grid, renewable energy integration, energy management, artificial intelligence, and embedded system design.

Baladev Biswal (Student Member, IEEE) received the B.Tech. degree in electrical engineering from the College of Engineering & Technology, Bhubaneswar, Odisha, India, in 2009 and the M.Tech. degree in power electronics from Motilal Nehru National Institute of Technology, Allahabad, India, in 2014, He is currently working toward the Ph.D. degree in electrical engineering with Siksha 'O' Anusandhan University, Bhubaneswar, Odisha, India.

His area of research includes ac and dc microgrid protection and control, renewable energy integration, signal processing, and artificial intelligence.

Eluri NVDV Prasad (Member, IEEE) received the B.E. degree from SIR CR Reddy College, Andhra University, Andhra Pradesh, India, in 2014, the M.Tech. degree in electrical and electronics engineering with power and industrial drives specialization from the GMRIT, JNTU Kakinada, Kakinada, India, in 2018, and the Ph.D. degree in electrical engineering from the from Siksha 'O' Anusandhan University, Odisha, India, in 2022.

He is currently working as an Assistant Professor with Sri Vasavi Engineering College, Tadepalligudem, AP, India. His area of research includes dc microgrid protection and control, HVdc protection, signal processing, and artificial intelligence.

Pradipta Kishore Dash (Life Senior Member, IEEE) received the B.E. and M.E. degrees in electrical engineering from the Indian Institute of Science, Bengaluru, India, in 1964, the Ph.D. degree in electrical engineering from Sambalpur University, Odisha, India, the Postdoctoral Education from the University of Calgary, Calgary, AB, Canada, in 1974 and 1976, respectively, and the D.Sc. degree in electrical engineering from Utkal University, Bhubaneswar, India, with a focus on AI and soft computing applications in power engineering, in 2003.

He is currently the Director (research and consultancy), Multidisciplinary Research Cell, Siksha 'O' Anusandhan University, Odisha, India. He has authored more than 500 research papers in reputed international journals and conferences in power systems, signal processing, renewable energy, computational intelligence, and data mining.

Sanjib Kumar Panda (Fellow, IEEE) received the B.Eng. degree from the South Gujarat University, Surat, India, in 1983, the M.Tech. degree from the Indian Institute of Technology, Banaras Hindu University, Varanasi, India, in 1987, and the Ph.D. degree from the University of Cambridge, Cambridge, U.K., in 1991, all in electrical engineering.

Since 1992, he has been holding a faculty position with the Department of Electrical and Computer Engineering, National University of Singapore, Singapore, where he is currently an Associate Professor and the Director of the Power & Energy Research Area. He has authored or coauthored more than 450 peer-reviewed research papers, coauthored one book, and contributed to several book chapters. He holds ten patents, and is the cofounder of three start-up companies. His research interests include high-performance control of motor drives and power electronic converters, condition monitoring and predictive maintenance, and building energy efficiency enhancement. He is an Associate Editor for IEEE TRANSACTIONS ON POWER ELECTRONICS, IEEE TRANSACTIONS ON INDUSTRY APPLICATIONS, IEEE TRANSACTIONS ON ENERGY CONVERSION, IEEE ACCESS, and IEEE JOURNAL OF EMERGING AND SELECTED TOPICS IN POWER ELECTRONICS. He is an IEEE PELS Distinguished Lecture for 2022–2023. He is the Chair of the IEEE PELS Technical Committee, TC-12: Energy Access and Off-grid Systems. Since 2016, he has also been the R-10 Membership & Chapter Development Coordinator for IEEE PELS since 2016.

Dr. Panda was the recipient of the Cambridge-Nehru Scholarship and the M. T. Mayer Graduate Scholarship during his Ph.D. study (1987–1991).